Canadian Science Publishing | Canadian Journal of Chemistry

Transient hypoxia in water irradiated by swift carbon ions at ultra-high dose rates: implication for FLASH carbon-ion therapy

Journal:	*Canadian Journal of Chemistry*
Manuscript ID	cjc-2021-0110
Manuscript Type:	Article
Date Submitted by the Author:	07-Apr-2021
Complete List of Authors:	Zakaria, Abdullah Muhammad; Université de Sherbrooke, Nuclear Medicine and Radiobiology Colangelo, Nicholas W.; Rutgers New Jersey Medical School, Radiology Meesungnoen, Jintana; Université de Sherbrooke, Nuclear Medicine and Radiobiology Jay-Gerin, Jean-Paul; Université de Sherbrooke, Médecine nucléaire et radiobiologie
Is the invited manuscript for consideration in a Special Issue? :	Not applicable (regular submission)
Keyword:	water radiolysis by swift carbon ions, Monte Carlo multi-track chemistry simulations, high absorbed dose rates, oxygen depletion, hydrogen peroxide formation, FLASH effect in carbon-ion radiotherapyy

Transient hypoxia in water irradiated by swift carbon ions at ultra-high dose rates: implication for FLASH carbon-ion therapy

by

Abdullah Muhammad Zakaria,[1,2] Nicholas W. Colangelo,[3] Jintana Meesungnoen,[1] and Jean-Paul Jay-Gerin[1,*]

[1] Département de Médecine Nucléaire et de Radiobiologie, Faculté de Médecine et des Sciences de la Santé, Université de Sherbrooke, 3001, 12ème Avenue Nord, Sherbrooke, QC J1H 5N4, Canada. E-mail: jean-paul.jay-gerin@USherbrooke.ca

[2] Present address: Quality Control Department, Knowlton Development Corporation, Knowlton, QC J0E 1V0, Canada.

[3] Rutgers Biomedical and Health Sciences, New Jersey Medical School, Department of Medicine, Newark, New Jersey, USA.

[*] Corresponding author.

Canadian Journal of Chemistry
Manuscript ID: cjc-2021-0110
May 25, 2021

Abstract:

Large doses of ionizing radiation delivered to tumors at ultra-high dose rates (*i.e.*, in a few milliseconds) paradoxically spare the surrounding healthy tissue while preserving anti-tumor activity (compared to conventional radiotherapy delivered at much lower dose rates). This new modality is known as "FLASH radiotherapy" (FLASH-RT). Although the molecular mechanisms underlying FLASH-RT are not yet fully understood, it has been suggested that radiation delivered at high dose rates spares normal tissue via oxygen depletion followed by subsequent radioresistance of the irradiated tissue. To date, FLASH-RT has been studied using electrons, photons and protons in various basic biological experiments, pre-clinical studies, and recently in a human patient. However, the efficacy of heavy ions, such as energetic carbon ions, under FLASH conditions remains unclear. Given that living cells and tissues consist mainly of water, we set out to study, from a pure radiation chemistry perspective, the effects of ultra-high dose rates on the transient yields and concentrations of radiolytic species formed in water irradiated by 300-MeV per nucleon carbon ions (LET ~ 11.6 keV/μm). This mimics irradiation in the "plateau" region of the depth-dose distribution of ions, *i.e.*, in the "normal" tissue region in which the LET is rather low. We used Monte Carlo simulations of multiple, simultaneously interacting radiation tracks together with an "instantaneous pulse" irradiation model. Our calculations show a pronounced oxygen depletion around 0.2 μs, strongly suggesting, as with electrons, photons and protons, that irradiation with energetic carbon ions at ultra-high dose rates is suitable for FLASH-RT.

Keywords: Liquid water, radiolysis, energetic carbon ions, absorbed dose rate, multiple track model, linear energy transfer (LET), Monte Carlo track chemistry simulations, oxygen depletion, hydrogen peroxide formation, FLASH effect, carbon-ion therapy.

1. Introduction

Radiation therapy uses ionizing radiation to treat cancer, and is part of the standard of care in oncology.[1] Around 50% of all cancer patients receive radiation therapy in the course of their illness. In addition, radiotherapy contributes towards 40% of curative cancer treatments.[2] In theory, all types of malignant tumors could be eradicated if treated with sufficiently high doses of radiation. However, the administration of curative doses of radiation is severely limited by acute and chronic toxicities to the normal tissue surrounding the tumor.[3]

It has recently been discovered that the delivery of ionizing radiation at ultra-high dose rates [*mean* dose rates greater than 40-100 Gy/s *vs.* ~0.03 Gy/s used in conventional radiotherapy (CONV-RT)] dramatically reduces almost instantly (within milliseconds) detrimental effects on healthy tissue while, paradoxically, maintaining the equivalent anti-tumor response of CONV-RT.[4-7] This fascinating new observation has been termed the "FLASH effect"[4] and its therapeutic application is called FLASH radiotherapy (FLASH-RT). Because of this immense potential clinical benefit, FLASH-RT has received considerable attention in the radiation oncology community, where FLASH-RT is considered "as one of the cancer breakthroughs of 2020".[8]

The phenomenon of cell sparing at very high dose rates has been known since the late 1960s,[9-15] but it is only recently that its clinical usefulness has attracted widespread attention. To date, FLASH-RT has been studied in animal models (*e.g.*, mice, mini-pigs and cats), pre-clinically *in vitro*[4,13-17] and even in a human patient.[18] The FLASH effect has so far been shown using predominantly dedicated electron linear accelerators (LINAC), and more recently with kilo-voltage energy X-rays[19,20] and cyclotron-based proton beams.[21-24]

Based on these recent reports on the relative protection of normal tissues, it appears promising to bring this new modality into clinical practice.[25] However, for full clinical implementation of this technique, new irradiators must be built to achieve these high dose rates.[26-28] Moreover, understanding the mechanisms by which tumors are selectively sterilized and normal tissue is spared by the FLASH effect is of the utmost importance to ensure that the effect is optimized while minimizing the risk of short- and long-term harm. This is a particularly urgent issue in FLASH-RT.[6,7,29-35]

While the exact molecular mechanisms behind FLASH-sparing of normal tissue are not well understood (for recent reviews, see **refs. 32-35**), a leading hypothesis is the radiolytic consumption (or "depletion") of the intracellular oxygen,[7,15,29,30,36-44] which cannot be replaced quickly enough by diffusion during the short radiation pulse time. In this proposed mechanism, FLASH creates a transient hypoxic environment in normal tissue, followed by subsequent radioresistance of the irradiated tissue.[45] At the same time, normal tissue may have a relative advantage over tumor cells. Tumors have a reduced ability to endogenously bind labile iron,[46] which *via* Fenton reactions contributes to the increase in the formation of free radicals. This increase in turn promotes oxidative stress and DNA damage in tumor tissue, compared to normal tissue.

Although the FLASH effect has so far been observed in the context of electron, photon and proton therapies, the question remains whether it can occur in therapy with heavy ions, such as energetic carbon ions.[47] Hadrontherapy has unique physical properties that allow more of the dose to be delivered to the tumor volume (*i.e.*, in the Bragg peak region) rather than normal tissue (*i.e.*, in the "plateau" region of the depth-dose distribution of ions).[48] It also offers increased relative biological effectiveness,[45,48-50] meaning that at a given dose of radiation, it kills tumor cells more efficiently than conventional radiation modalities. From a radiobiological perspective, normal tissue sparing effects associated with hadrontherapy and FLASH-RT might be additive or even

synergistic.[47] Unfortunately, there are no published studies that show whether the tissue-sparing FLASH effect can be achieved in hadrontherapy and, in particular, in carbon-ion therapy. Monte Carlo simulations can therefore improve our physicochemical understanding of why carbon ions may be suitable for FLASH-RT.[47,51] Such data are important and necessary as the use of carbon-ion beams in radiotherapy increases worldwide.

Since fundamental radiobiological processes are usually triggered in an aqueous environment (living cells and tissues consist of ~70-85% water by weight), a thorough knowledge of water radiolysis[52-54] is certainly relevant for the general understanding of the FLASH effect. Here we study from a pure radiation chemistry perspective the effects of high dose rates on the transient yields (*G* values) and the corresponding concentrations of radiolytic species formed in liquid water that is irradiated with energetic carbon ions. To achieve this, we use Monte Carlo simulations of multiple, simultaneously interacting radiation tracks together with an "instantaneous pulse" irradiation model previously developed by our group[44] for the low "linear energy transfer" (LET) case of 300-MeV incident protons (LET ~ 0.3 keV/μm at 25 °C). Our main focus is on quantifying the effect of the radiolytic process on oxygen consumption (depletion) and hydrogen peroxide formation by high-LET carbon ion irradiation at high dose rates induced in the time window ~ps–ms; processes that are relevant for FLASH-RT.

2. The FLASH effect: Water radiolysis and the oxygen depletion hypothesis

At this point it should be briefly recalled that in ~1 ps after initial energy deposition, radiolytic products formed in irradiated pure liquid water[54] include the hydrated electron (e^-_{aq}), $H^\bullet$, H_2, $^\bullet OH$, H_2O_2, H_3O^+, OH^-, *etc*. Of these, the e^-_{aq} and $^\bullet OH$ radicals are produced in the highest concentrations, and $^\bullet OH$ is considered the most harmful from a

radiobiological point of view.[55] In an aerobic cellular environment, e^-_{aq} and $H^\bullet$ atoms are scavenged by dissolved molecular oxygen in the microsecond time scale (assuming a typical intracellular O_2 concentration of ~30 μM) and converted into superoxide anion radicals ($O_2^{\bullet-}$):[56,57]

(1) $e^-_{aq} + O_2 \rightarrow O_2^{\bullet-}$ $k_1 = 2.3 \times 10^{10}$ M^{-1} s^{-1}

(2) $H^\bullet + O_2 \rightarrow HO_2^\bullet$ $k_2 = 1.3 \times 10^{10}$ M^{-1} s^{-1}

where $O_2^{\bullet-}$ is always in a pH-dependent equilibrium with its conjugate acid, the hydroperoxyl radical $HO_2^\bullet$ [$pK_a(HO_2^\bullet/O_2^{\bullet-}) \approx 4.8$ in water at 25 °C[56]].

(3) $HO_2^\bullet$ ϵ $O_2^{\bullet-} + H^+$

As mentioned in the Introduction, it is becoming increasingly evident that the radiation-chemical depletion (consumption) of tissue oxygen contributes – at least partially – to the FLASH effect, although the extent of its contribution remains unknown and warrants further investigation.[32]

Oxygen depletion in response to high dose-rate irradiations occurs whenever its replenishment by diffusion is inefficient, which commonly occurs when O_2-containing systems are irradiated.[58] The question of interest here is the timescale of oxygen depletion versus reoxygenation. Under normal conditions, approximately 98.5% of the oxygen in the blood is bound to hemoglobin ($Hb–O_2$) and transported from the lungs to peripheral tissues. The dissociation of oxygen from hemoglobin occurs on the timescale of tens of milliseconds. However, as illustrated in Fig. 1, it takes about 1 s for oxygen to diffuse from the blood vessel to the irradiated cells at a distance of ~100 μm (assuming a value of 2.4×10^{-9} m^2 s^{-1} for the diffusion coefficient of O_2 in water[59]), effectively preventing O_2 from reoxygenating these oxygen-depleted areas during the ultrashort FLASH exposure.[36-38,60]

Various chemical pathways have been proposed to explain the transient radiolytic oxygen depletion during FLASH irradiation. These include (for a recent critical review, see **ref. 58**):

- Reactions (1) and (2) of e^-_{aq} and $H^\bullet$ with O_2, yielding superoxide radicals. The superoxide dismutase (SOD)-catalyzed dismutation of $O_2^{\bullet-}$ will partially re-supply O_2 in the cells as well as produce H_2O_2:[56,61]

(4) $O_2^{\bullet-} + O_2^{\bullet-} + (2H^+) \xrightarrow{SOD} H_2O_2 + O_2 \quad k_4 \approx 4 \times 10^9\ M^{-1}\ s^{-1}$

$HO_2^\bullet/O_2^{\bullet-}$ can also react quickly with $^\bullet OH$ radicals to give O_2 alone:

(5) $HO_2^\bullet + {}^\bullet OH \rightarrow O_2 + H_2O \quad k_5 = 9 \times 10^9\ M^{-1}\ s^{-1}$

(6) $O_2^{\bullet-} + {}^\bullet OH \rightarrow O_2 + OH^- \quad k_6 = 1.1 \times 10^{10}\ M^{-1}\ s^{-1}$

and with nitric oxide ($^\bullet NO$) generated in large amounts in exposed cells,[62] to form the peroxynitrite anion ($ONOO^-$):

(7) $O_2^{\bullet-} + {}^\bullet NO \rightarrow ONOO^- \quad k_7 = 1.9 \times 10^{10}\ M^{-1}\ s^{-1}$.

$ONOO^-$ and its conjugate acid, peroxynitrous acid ($ONOOH/ONOO^-$, pK_a = 6.8 at 37 °C), are powerful and toxic (non-radical) oxidizing agents;

- Addition of O_2 to carbon-centered radicals ($R^\bullet$), most often formed by $H^\bullet$-atom abstraction from organic substrates (RH) (*e.g.*, initiated by $^\bullet OH$ radicals released by water radiolysis), yielding peroxyl radicals $ROO^\bullet$.[39,40] These $ROO^\bullet$ radicals, which are stronger oxidizing agents than their parent radicals,[63] can initiate membrane lipid peroxidation chain reactions that increase O_2 consumption and release organic hydroperoxides (ROOH).[55,57]

Regardless of the relative contribution of the various proposed mechanisms, a better quantitative understanding of these early physicochemical events which occur

immediately after the formation of water radiolysis products is critical to determining the essential parameters of the FLASH modality and whether FLASH techniques can impact hadrontherapy, such as therapy with carbon ions.

3. Multi-track model for dose-rate effects: Monte Carlo simulations

Assuming that cells can be modeled as pure, air-saturated water, our group[44] recently developed an irradiation model to study the effects of high dose rates on the radiolysis of water by 300-MeV incident protons, which mimic the low-LET of ^{60}Co γ rays or a beam of energetic (*e.g.*, MeV) electrons. In the present work, we have adapted this model for the case of irradiation with swift carbon ions. In short, the model consists of the random irradiation of water with single and instantaneous pulses[64] of N incident 300-MeV per nucleon $^{12}C^{6+}$ ions (LET ~ 11.6 keV/μm at 25 °C),[65,66] which penetrate this water perpendicularly across the surface of a circle with radius R_o (Fig. 2). This model mimics irradiation in the "plateau" region of the depth-dose distribution of ions,[48] *i.e.*, in the entrance channel that corresponds to the "normal" tissue region in which the LET is rather low. An advantage of using energetic carbon ions is that their trajectories are essentially rectilinear, which makes it possible to define a cylindrical geometry of the beam at the time of entry. In this geometry, the carbon ion tracks run parallel to the cylinder axis. The tracks initially contained in this cylinder are obviously not restricted to this volume, but develop over time throughout the entire solution via the diffusion of the various radiolytic species that were initially formed in it. This problem is very similar to the one we have dealt with for many years in Monte Carlo simulations of the radiolysis of water. However, instead of simulating a single carbon ion track at a time (limit of low dose rate),[67] we simulate N interactive tracks simultaneously. Under these conditions, *the effect of the dose rate is studied by simply varying N*.

Our Monte Carlo track-chemistry computer code IONLYS-IRT[54] was used to simulate the radiolysis of liquid water by 300-MeV per nucleon irradiating carbon ions. A detailed description of this code at ambient temperature has been reported elsewhere.[51,54,68-71] In short, our code first models the early *physical and physicochemical stages* of the radiation action up to ~1 ps in track development in a 3D geometric environment ("IONLYS" program). At the relatively low dose rates used in conventional radiotherapy, the distance between the individual tracks is so great that they can be regarded as isolated. In such a situation, the history of only one single track needs to be considered, and the radiolysis yields are independent of the dose rate. As the dose rate increases, however, so does the number of localized tracks present at the same time, as a result of which the average distance between the neighboring tracks decreases. These dose-rate effects set in when the distance between ionization events becomes sufficiently small and interactions occur between the various incident tracks. Since our program can only simulate the spatio-temporal history of one carbon ion track at a time, we have modified it so that simultaneously incident tracks in close spatial proximity can be calculated.[44] In this study, the number of impacting $^{12}C^{6+}$ ions per pulse was chosen so that it varied from $N = 1$ (low dose rate limit) to 75 (the maximum achievable value given our computing capacity). These N carbon ions reach the front of the cylinder at the same time (chosen as time zero) and travel parallel to the positive Y-axis (Fig. 2).

The complex spatial distribution of the reactants of the considered track system at the end of the physicochemical stage is provided as an output of the IONLYS program. It is then used directly as the starting point for the subsequent *chemical stage* (>1 ps). Here, the various radiolytic species randomly diffuse at rates determined by their diffusion coefficients and react with each other or in competition with dissolved solutes (O_2 in the case studied here) present in the solution at the time of irradiation. This third

stage is covered by our “IRT” program, which uses the “independent reaction times” or IRT method,[69,72,73] a computationally efficient stochastic simulation technique that simulates reaction times without having to follow the trajectories of the diffusing species. Its implementation has been described elsewhere.[44,69] The ability of this method to give accurate time-dependent chemical yields over a wide range of irradiation conditions has been well validated by comparison to full random flight (or step-by-step) Monte Carlo simulations,[74,75] which follow the trajectories of the reactants in detail. While the consideration of a large number of carbon ion trajectories for the implementation of our IRT program at high dose rates was not a particular problem, the only disadvantage here was that the computation times were obviously longer than for the simulation of single trajectories.

The main reaction scheme and rate constants, as well as the diffusion coefficients of reactive species used in our IRT program for aerated and deaerated irradiated water at 25 °C, are the same as those used previously, as described elsewhere.[59,69,76,77] The concentration of dissolved oxygen is taken to be 0.25 mM (“air-saturated” water).

All calculations were performed by simulating short (~3–30 μm, depending on *N*) segments of 300-MeV per nucleon irradiating $^{12}C^{6+}$ ion tracks. The energy and LET of the carbon ions are well defined over these simulated track segments and remain nearly constant and equal to ~11.6 keV/μm. For a given value of *N*, the number of simulation “histories” was chosen to ensure only minor statistical fluctuations in the calculated average chemical yields while maintaining acceptable computer time limits.

In this article, *G*-values are given in units of molecules formed or consumed per 100 eV of radiation energy absorbed. For conversion into SI units, 1 molecule/100 eV ≈ 0.10364 μmol/J.[52,53]

4. Results and discussion

Figure 3 shows the temporal variation of the yield of consumed oxygen, $G(-O_2)$, parameterized by a few values of N between 1 and 75, as obtained from our simulations of the radiolysis of aerated water by 300-MeV per nucleon $^{12}C^{6+}$ ions at 25 °C, in the interval ~1 ps–10 μs. Data for N = 1 indicating the limit of low dose rates (*i.e.*, with no overlap between the tracks of different incident carbon ions) are used as a reference. As expected, $G(-O_2)$ remains equal to zero at early times until dissolved O_2 begins to react with e^-_{aq} and $H^\bullet$ via reactions (1) and (2). In this case $G(-O_2)$ increases rapidly for all values of N, reaches a maximum around one microsecond (*i.e.*, when all e^-_{aq} and $H^\bullet$ atoms have been scavenged), and then slowly decreases. This decrease in $G(-O_2)$ at times longer than ~1 μs is dominated by the secondary reactions (5) and (6) of $HO_2^\bullet/O_2^{\bullet-}$ with $^\bullet$OH radicals. These results are shown in Fig. 4A-B, in which, for N = 10 and 75, we compare the cumulative yield variations, $\Delta G(-O_2)$, for each of the reactions that contribute to the formation and consumption of oxygen.

An important result of Fig. 3 is the substantial decrease in the maximum of $G(-O_2)$, which drops from ~2.15 to 0.85 molecules per 100 eV as N increases from 1 to 75. This indicates that as N (*i.e.*, the dose rate) increases, the probability of intertrack reactions in the bulk of the solution increases leading to greater competition between radical-radical reactions and radical-solute (*i.e.*, O_2 in the present case) reactions. In other words, an increasing number of e^-_{aq} and $H^\bullet$ atoms in the track stage of radiolysis are involved in inter-radical reactions *before* they even have a chance to react with O_2.[44,78]

Using the irradiation model from Fig. 2 and the $G(-O_2)$ values obtained from our Monte Carlo simulations, the consumed oxygen concentrations, $[-O_2]$, can simply be derived from the general relationship:[44,79]

(8) $C = \rho \mathcal{D} G$,

where C is the concentration, ρ is the density of the solution, $\mathcal{D}$ is the radiation dose and G is the chemical yield. Assuming that the O_2 molecules in the considered circular cylinder with a length of 1 μm and an initial radius R_o = 0.1 μm (at ~1 ps; see Fig. 2) are evenly consumed, [–O_2] (expressed in mM) can then be written in this case as

$$(9)\quad [{-}O_2](t) \approx 5.3 \times 10^{-6} \times \left(\frac{N \times \mathrm{LET}}{R(t)^2} \right) \times G({-}O_2)(t),$$

where LET ≈ 11.6 keV/μm for 300-MeV per nucleon irradiating carbon ions, G(–O_2) is in molecules per 100 eV, and

$$(10)\quad R(t)^2 \approx R_o^2 + 4Dt$$

represents the change in R_o (in μm) over time due to the two-dimensional diffusive expansion of the tracks. Here, t is the time and D is the diffusion coefficient of the various track species involved in our IRT simulations.[80]

Figure 5 shows the time profile of [–O_2] at 25 °C in the interval of ~1 ps –10 μs, estimated directly from Eqs. (9) and (10) for N between 1 and 75, using the G(–O_2) values given in Fig. 3. As can be seen, [–O_2] first increases at approximately one nanosecond to reach a maximum around 0.2 μs, and then decreases towards zero after about 10 μs (depending on N). This maximum is not very pronounced or even almost absent for values of N < 10. However, it increases markedly with increasing dose rate, reaching a value of ~0.22 mM for N = 75, the highest dose rate studied in this work. Despite the model's simplicity, these results strongly suggest that oxygen depletion can be induced by high-dose-rate irradiation with energetic carbon ions, similar to our previous study with protons.[44]

Let us recall here that for pulses of N = 2000 300-MeV incident protons (LET ~ 0.3 keV/μm) and an irradiation geometry identical to that used in this work,[44] a major part of

the available oxygen was consumed for dose rates close to 10^{10} Gy/s. Interestingly, similar results are obtained for pulses of N = 75 300-MeV per nucleon incident carbon ions (LET ~ 11.6 keV/μm). In fact, the product ($N \times$ LET) in Eq. (9), which represents the energy initially deposited in the irradiation cylinder of Fig. 1 is roughly the same in both cases. We can, therefore, conclude that pulses of N = 75 300-MeV per nucleon carbon ions correspond to a dose rate of ~10^{10} Gy/s in our model system.

Assuming that the tissue sparing in FLASH-RT is, indeed, due to the depletion of oxygen in cells, then the transient, radiolytic oxygen depletion found in this work indicates that irradiation with carbon ions at high dose rates, as with electrons, photons or protons, is suitable for FLASH-RT and, thus, could be implemented in carbon-ion therapy.

Even if the bio-mimetic use of pure water as a model for studying H_2O_2 generation in irradiated tissue may be questioned,[58] the yields of H_2O_2 produced in the carbon ion radiolysis of aerated and deaerated water for different values of N (*i.e.*, the dose rate) are of great interest from a pure water radiation chemistry point of view. Figure 6 shows our simulated time-dependent $G(H_2O_2)$ values for 300-MeV per nucleon irradiating carbon ions and for various values of N between 1 and 50, which were chosen as examples. As can be seen, in the presence of oxygen, there is an increase in H_2O_2 production at times longer than a hundred nanoseconds compared to the normal radiolytic H_2O_2, which is generated in the absence of oxygen via the self-reaction of the hydroxyl radical:[52,53,77]

(11) $^{\bullet}OH + {}^{\bullet}OH \rightarrow H_2O_2 \quad k_{11} = 4.8 \times 10^9\ M^{-1}\ s^{-1}$.

As previously discussed in Sect. 2, this additional H_2O_2 production in irradiated aerated water results from the intervention of reactions (1) and (2) and the subsequent secondary $O_2^{\bullet-}$ and $HO_2^{\bullet}$ radical reactions,[56] such as reaction (4). It is also interesting

to see from Fig. 6 that as dose-rate effects develop, the H_2O_2 yield increases with the dose rate for both aerated and deaerated water. This result agrees with the general scheme[52] that an increase in the dose rate leads to an increase in the radical densities, which in turn leads to a greater proportion of inter-track radical-radical reactions which favor an increase in the molecular product yields in the system as a whole.

Finally, using Eqs. (9) and (10) where [$-O_2$] and $G(-O_2)$ are replaced by [H_2O_2] and $G(H_2O_2)$, we can estimate the corresponding concentration of H_2O_2 as a function of time for N = 1, 5, 10, 50 and 75 irradiating carbon ions per pulse. This is shown in Fig. 7. As can be seen, [H_2O_2] shows a broad maximum around 30 ns, which increases substantially with increasing values of N, going from ~5 μM for N = 1 to ~0.36 mM for N = 75 (*i.e.*, for a dose rate of about 10^{10} Gy/s). Interestingly, this increase in [H_2O_2] at high dose rates is in apparent contradiction to a recently published report[15] indicating that FLASH produces lower levels of H_2O_2 in irradiated cells. However, it is difficult to reliably compare those experimental results and our calculations. First, the authors[15] did not specify the time of their H_2O_2 measurements after irradiation (but which could possibly be relatively long, perhaps several minutes or more). Second, our calculations concern the radiolysis of pure, aerated water, not of irradiated cells. As discussed recently,[58] the presence of high concentrations of radical scavengers in cells should likely lead to rapid catalytic destruction of H_2O_2 with the result that much lower levels of H_2O_2 are produced compared to those calculated in this work for pure water.

However, as the dose rate increases, Fenton-type chain reactions in tumor tissues exposed to FLASH-RT are greatly intensified by the subsequent increase in the H_2O_2 concentration (compared to normal tissue, which can regulate endogenous levels of labile Fe more effectively). This leads to higher levels of organic hydroperoxides and oxidative damage in cancer cells.

5. Conclusion

In this study, we investigated the impact of high-dose-rate effects on the radiolysis of water by swift carbon ions from a purely radiation chemistry perspective. Monte Carlo simulations of multiple, simultaneously interacting radiation tracks were used along with a cylindrical, "instantaneous pulse" irradiation model to quantify the effect of the radiolytic processes on O_2 consumption and H_2O_2 formation induced in the ~ps–ms time window by 300-MeV per nucleon carbon ions (LET ~ 11.6 keV/μm).

We found a substantial increase in the concentration of consumed (depleted) oxygen with increasing dose rate, reaching almost 90% of the oxygen present in the solution for N = 75, the highest dose rate (estimated to ~10^{10} Gy/s) studied in this work. Our results suggest that temporary hypoxia due to the radiolytic O_2 depletion can be induced by carbon ions at FLASH dose rates, similar to previous studies with electrons, photons and protons.

As expected, the increase in the density of primary events at high dose rates favors the occurrence of inter-track radical-radical combination/recombination reactions, thus leading to lower radical and higher molecular yields. Our results for hydrogen peroxide tend to follow this general pattern. Interestingly, our calculated H_2O_2 concentrations at high dose rates appear to contradict some experimental data, which indicates that FLASH produces lower levels of H_2O_2 in cells irradiated under these conditions.

Finally, our results suggest that by integrating FLASH techniques with carbon-ion therapy, an even better therapeutic ratio is achieved in the tumor (*i.e.*, at the Bragg peak near the end of the ion range), thereby increasing cell-killing efficacy[47,51] while simultaneously protecting normal tissue (*i.e.*, in the entrance "plateau" region). Of course, these findings need to be tested experimentally to determine the early physicochemical events at ultra-high dose rates and to confirm the proposed underlying mechanisms of the remarkable biological effects of FLASH-RT.

Acknowledgements

A.M.Z. is the recipient of an M.Sc. scholarship from the “Programme de Bourses d’excellence aux études supérieures” of the Université de Sherbrooke. The authors gratefully acknowledge Professor Edouard I. Azzam, Dr. Manuela Buonanno, Dr. Vincent Favaudon, and Dr. Jean Cadet for helpful discussions and stimulating correspondence. The research of J.-P. J.-G. is supported by the Natural Sciences and Engineering Research Council of Canada (NSERC) Discovery Grant No. RGPIN-2015-06100.

References

(1) Halperin, E. C.; Brady, L. W.; Perez, C. A.; Wazer, D. E. *Perez & Brady's Principles and Practice of Radiation Oncology*; Lippincott Williams & Wilkins: Philadelphia, PA, 2013.

(2) Baskar, R.; Lee, K. A.; Yeo, R.; Yeoh, K.-W. *Int. J. Med. Sci.* **2012**, *9*, 193.

(3) Bernier, J.; Hall, E. J.; Giaccia, A. *Nat. Rev. Cancer* **2004**, *4*, 737.

(4) Favaudon, V.; Caplier, L.; Monceau, V.; Pouzoulet, F.; Sayarath, M.; Fouillade, C.; Poupon, M.-F.; Brito, I.; Hupé, P.; Bourhis, J.; Hall, J.; Fontaine, J.-J.; Vozenin, M.-C. *Sci. Transl. Med.* **2014**, *6*, 245ra93.

(5) Favaudon, V.; Fouillade, C.; Vozenin, M.-C. *Cancer Radiother.* **2015**, *19*, 526.

(6) Favaudon, V. *Cancer Radiother.* **2019**, *23*, 674.

(7) Vozenin, M.-C.; Hendry, J. H.; Limoli, C. L. *Clin. Oncol.* **2019**, *31*, 407.

(8) Freeman, T. *Physics World*. IOP Publishing Ltd. (6 August 2019). Website: physicsworld.com/a/flash-radiotherapy-from-preclinical-promise-to-the-first-human-treatment/

(9) Hornsey, S.; Alper, T. *Nature* **1966**, *210*, 212.

(10) Town, C. D. *Nature* **1967**, *215*, 847.

(11) Berry, R. J.; Hall, E. J.; Forster, D. W.; Storr, T. H.; Goodman, M. J. *Br. J. Radiol.* **1969**, *42*, 102.

(12) Epp, E. R.; Weiss, H.; Ling, C. C. *Curr. Top. Radiat. Res. Q.* **1976**, *11*, 201.

(13) Montay-Gruel, P.; Petersson, K.; Jaccard, M.; Boivin, G.; Germond, J.-F.; Petit, B.; Doenlen, R.; Favaudon, V.; Bochud, F.; Bailat, C.; Bourhis, J.; Vozenin, M.-C. *Radiother. Oncol.* **2017**, *124*, 365.

(14) Vozenin, M.-C.; de Fornel, P.; Petersson, K.; Favaudon, V.; Jaccard, M.; Germond, J.-F.; Petit, B.; Burki, M.; Ferrand, G.; Patin, D.; Bouchaad, H.; Ozsahin, M.; Bochud, F.; Bailat, C.; Devauchelle, P.; Bouhris, J. *Clin. Cancer Res.* **2019**, *25*, 35.

(15) Montay-Gruel, P.; Acharya, M. M.; Petersson, K.; Alikhani, L.; Yakkala, C.; Allen, B. D.; Ollivier, J.; Petit, B.; Jorge, P. G.; Syage, A. R.; Nguyen, T. A.; Baddour, Al A. D.; Lu, C.; Singh, P.; Moeckli, R.; Bochud, F.; Germond, J.-F.; Froidevaux, P.; Bailat, C.; Bourhis, J.; Vozenin, M.-C.; Limoli, C. L. *Proc. Natl. Acad. Sci. USA* **2019**, *116*, 10943.

(16) Simmons, D. A.; Lartey, F. M.; Schuler, E.; Rafat, M.; King, G.; Kim, A.; Ko, R.; Semaan, S.; Gonzalez, S.; Jenkins, M.; Pradhan, P.; Shih, Z.; Wang, J.; von Eyben, R.; Graves, E. E.; Maxim, P. G.; Longo, F. M.; Loo, B. W., Jr. *Radiother. Oncol.* **2019**, *139*, 4.

(17) Soto, L. A.; Casey, K. M.; Wang, J.; Blaney, A.; Manjappa, R.; Breitkreutz, D.; Skinner, L.; Dutt, S.; Ko, R. B.; Bush, K.; Yu, A. S.; Melemenidis, S.; Strober, S.; Englemann, E.; Maxim, P. G.; Graves, E. E.; Loo, B. W. Jr. *Radiat. Res.* **2020**, *194*, 618.

(18) Bourhis, J.; Jeanneret-Sozzi, W.; Jorge, P. G.; Gaide, O.; Bailat, C.; Duclos, F.; Patin, D.; Ozsahin, M.; Bochud, F.; Germond, J.-F.; Moeckli, R.; Vozenin, M.-C. *Radiother. Oncol.* **2019**, *139*, 18.

(19) Montay-Gruel, P.; Bouchet, A.; Jaccard, M.; Patin, D.; Serduc, R.; Aim, W.; Petersson, K.; Petit, B.; Bailat, C.; Bourhis, J.; Bräuer-Krisch, E.; Vozenin, M.-C. *Radiother. Oncol.* **2018**, *129*, 582.

(20) Eling, L.; Bouchet, A.; Nemoz, C.; Djonov, V.; Balosso, J.; Laissue, J.; Bräuer-Krisch, E.; Adam, J.-F.; Serduc, R. *Radiother. Oncol.* **2019**, *139*, 56.

(21) van de Water, S.; Safai, S.; Schippers, J. M.; Weber, D. C.; Lomax, A. J. *Acta Oncol.* **2019**, *58*, 1463.

(22) Buonanno, M.; Grilj, V.; Brenner, D. J. *Radiother. Oncol.* **2019**, *139*, 51.

(23) Grilj, V.; Buonanno, M.; Welch, D.; Brenner, D. J. *Radiat. Res.* **2020**, *194*, 646.

(24) Diffenderfer, E. S.; Verginadis, I. I.; Kim, M. M.; Shoniyozov, K.; Velalopoulou, A.; Goia, D.; Putt, M.; Hagan, S.; Avery, S.; Teo, K.; Zou, W.; Lin, A.; Swisher-McClure, S.; Koch, C.; Kennedy, A. R.; Minn, A.; Maity, A.; Busch, T. M.; Dong, L.; Koumenis, C.; Metz, J.; Cengel, K. A. *Int. J. Radiat. Oncol. Biol. Phys.* **2020**, *106*, 440.

(25) Bourhis, J.; Montay-Gruel, P.; Jorge, P. G.; Bailat, C.; Petit, B.; Ollivier, J.; Jeanneret-Sozzi, W.; Ozsahin, M.; Bochud, F.; Moeckli, R.; Germond, J.-F.; Vozenin, M.-C. *Radiother. Oncol.* **2019**, *139*, 11.

(26) Schüler, E.; Trovati, S.; King, G.; Lartey, F.; Rafat, M.; Villegas, M.; Praxel, A. J.; Loo, B. W., Jr.; Maxim, P. G. *Int. J. Radiat. Oncol. Biol. Phys.* **2017**, *97*, 195.

(27) Lempart, M.; Blad, B.; Adrian, G.; Bäck, S.; Knöös, T.; Ceberg, C.; Petersson, K. *Radiother. Oncol.* **2019**, *139*, 40.

(28) Favaudon, V.; Lentz, J.-M.; Heinrich, S.; Patriarca, A.; de Marzi, L.; Fouillade, C.; Dutreix, M. *Nucl. Instrum. Methods Phys. Res. A* **2019**, *944*, 162537.

(29) Durante, M.; Bräuer-Krisch, E.; Hill, M. *Br. J. Radiol.* **2018**, *91*, 20170628.

(30) Boscolo, D.; Krämer, M.; Fuss, M. C.; Durante, M.; Scifoni, E. *Int. J. Mol. Sci.* **2020**, *21*, 424.

(31) Harrington, K. J. *Clin. Cancer Res.* **2019**, *25*, 3.

(32) Wilson, J. D.; Hammond, E. M.; Higgins, G. S.; Petersson, K. *Front. Oncol.* **2020**, *9*, 1563.

(33) Griffin, R. J.; Ahmed, M. M.; Amendola, B.; Belyakov, O.; Bentzen, S. M.; Butterworth, K. T.; Chang, S.; Coleman, C. N.; Djonov, V.; Formenti, S. C.; Glatstein, E.; Guha, C.; Kalnicki, S.; Le, Q.-T.; Loo, B. W., Jr.; Mahadevan, A.; Massaccesi, M.; Maxim, P. G.; Mohiuddin, M.; Mohiuddin, M.; Mayr, N. A.; Obcemea, C.; Petersson, K.; Regine, W.; Roach, M.; Romanelli, P.; Simone 2nd, C. B.; Snider, J. W.; Spitz, D. R.; Vikram, B.; Vozenin, M.-C.; Abdel-Wahab, M.; Welsh, J.; Wu, X.; Limoli, C. L. *Int. J. Radiat. Oncol. Biol. Phys.* **2020**, *107*, 766.

(34) de Kruijff, R. M. *Int. J. Radiat. Biol.* **2020**, *96*, 419.

(35) Hughes, J. R.; Parsons, J. L. *Int. J. Mol. Sci.* **2020**, *21*, 6492.

(36) Pratx, G.; Kapp, D. S. *Phys. Med. Biol.* **2019**, *64*, 185005.

(37) Pratx, G.; Kapp, D. S. *Int. J. Radiat. Oncol. Biol. Phys.* **2019**, *105*, 190.

(38) Khan, S.; Bassenne, M.; Wang, J.; Manjappa, R.; Melemenidis, S.; Breitkreutz, D. Y.; Maxim, P. G.; Xing, L.; Loo, B. W., Jr.; Pratx, G. *Int. J. Radiat. Oncol. Biol. Phys.* **2021**. DOI: 10.1016/j.ijrobp.2021.01.050

(39) Spitz, D. R.; Buettner, G. R.; Petronek, M. S.; St-Aubin, J. J.; Flynn, R. T.; Waldron, T. J.; Limoli, C. L. *Radiother. Oncol.* **2019**, *139*, 23.

(40) Labarbe, R.; Hotoiu, L.; Barbier, J.; Favaudon, V. *Radiother. Oncol.* **2020**, *153*, 303.

(41) Adrian, G.; Konradsson, E.; Lempart, M.; Bäck, S.; Ceberg, C.; Petersson, K. *Br. J. Radiol.* **2020**, *93*, 20190702.

(42) Petersson, K.; Adrian, G.; Butterworth, K.; McMahon, S. J. *Int. J. Radiat. Oncol. Biol. Phys.* **2020**, *107*, 539.

(43) Abolfath, R.; Grosshans, D.; Mohan, R. *Med. Phys.* **2020**, *47*, 6551.

(44) Alanazi, A.; Meesungnoen, J.; Jay-Gerin, J.-P. *Radiat. Res.* **2021**, *195*, 149.

(45) Hall, E. J.; Giaccia, A. J. *Radiobiology for the Radiologist*, 8th ed.; Wolters Kluwer: Philadelphia, PA, 2019.

(46) Jung, M.; Mertens, C.; Tomat, E.; Brüne, B. *Int. J. Mol. Sci.* **2019**, *20*, 273.

(47) Colangelo, N. W.; Azzam, E. I. *Radiat. Res.* **2020**, *193*, 1.

(48) Schardt, D.; Elsässer, T.; Schulz-Ertner, D. *Rev. Mod. Phys.* **2010**, *82*, 383.

(49) Schlaff, C. D.; Krauze, A.; Belard, A.; O'Connell, J. J.; Camphausen, K. A. *Radiat. Oncol.* **2014**, *9*, 88.

(50) Tinganelli, W.; Durante, M. *Cancers* **2020**, *12*, 3022.

(51) Zakaria, A. M.; Colangelo, N. W.; Meesungnoen, J.; Azzam, E. I.; Plourde, M.-É.; Jay-Gerin, J.-P. *Radiat. Res.* **2020**, *194*, 587.

(52) Spinks, J. W. T.; Woods, R. J. *An Introduction to Radiation Chemistry*, 3rd ed.; Wiley: New York, NY, 1990.

(53) Ferradini, C.; Jay-Gerin, J.-P. *Can. J. Chem.* **1999**, *77*, 1542.

(54) Meesungnoen, J.; Jay-Gerin, J.-P. *Charged particles and photon interactions with matter. Recent advances, applications, and interfaces*; Hatano, Y.; Katsumura, Y.; Mozumder, A.; Eds.; Taylor & Francis: Boca Raton, FL, 2011; pp. 355–400.

(55) von Sonntag, C. *Free-Radical-Induced DNA Damage and its Repair. A Chemical Perspective*; Springer-Verlag: Berlin, 2006.

(56) Bielski, B. H.; Cabelli, D. E.; Arudi, R. L.; Ross, A. B. *J. Phys. Chem. Ref. Data* 1985, **14**, 1041.

(57) Azzam, E. I.; Jay-Gerin, J.-P.; Pain, D. *Cancer Lett.* **2012**, *327*, 48.

(58) Wardman, P. *Radiat. Res.* **2020**, *194*, 607.

(59) Tippayamontri, T.; Sunuchakan, S.; Meesungnoen, J.; Sunaryo, G. R.; Jay-Gerin, J.-P. In *Recent Research Developments in Physical Chemistry*; Pandalai, S. G.;

Ed.; Transworld Research Network: Trivandrum, Kerala, India, 2009; vol. 10, pp. 143–211.

(60) Wilson, P.; Jones, B.; Yokoi, T.; Hill, M.; Vojnovic, B. *Br. J. Radiol.* **2012**, *85*, e933.

(61) Jay-Gerin, J.-P.; Ferradini, C. *Biochimie* **2000**, *82*, 161.

(62) Mikkelsen, R. B.; Wardman, P. *Oncogene* **2003**, *22*, 5734.

(63) Alfassi, Z. B. (Ed.), *Peroxyl Radicals*; Springer: Berlin, 1997.

(64) This is the so-called model of the “instantaneous pulse” in which the pulse duration is assumed to be zero. See, for example, *The Dosimetry of Pulse Radiation*, ICRU Report No. 34; International Commission on Radiation Units and Measurements: Bethesda, MD, 1982.

(65) Watt, D. E. *Quantities for Dosimetry of Ionizing Radiations in Liquid Water*; Taylor & Francis: London, UK, 1996.

(66) There are currently around fifteen centers worldwide treating with carbon-ion therapy. The therapeutic carbon-ion beams used cover an energy range generally between 100 and 400 MeV per nucleon. For example, see **ref. 50**.

(67) Alanazi, A.; Meesungnoen, J.; Jay-Gerin, J.-P. *Can. J. Chem.* **2020**, *98*, 427.

(68) Cobut, V.; Frongillo, Y.; Patau, J. P.; Goulet, T.; Fraser, M.-J.; Jay-Gerin, J.-P. Radiat. Phys. Chem. **1998**, *51*, 229.

(69) Frongillo, Y.; Goulet, T.; Fraser, M.-J.; Cobut, V.; Patau, J. P.; Jay-Gerin, J.-P. *Radiat. Phys. Chem.* **1998**, *51*, 245.

(70) Meesungnoen, J.; Jay-Gerin, J.-P. *J. Phys. Chem. A* **2005**, *109*, 6406.

(71) Meesungnoen, J.; Jay-Gerin, J.-P. *Radiat. Res.* **2009**, *171*, 379.

(72) Tachiya, M. *Radiat. Phys. Chem.* **1983**, *21*, 167.

(73) Pimblott, S. M.; Pilling, M. J.; Green, N. J. B. *Radiat. Phys. Chem.* **1991**, *37*, 377.

(74) Goulet, T.; Fraser, M.-J.; Frongillo, Y.; Jay-Gerin, J.-P. *Radiat. Phys. Chem.* **1998**, *51*, 85.

(75) Plante, I. Ph.D. thesis, Université de Sherbrooke, Sherbrooke, Que., 2009.

(76) Mirsaleh Kohan, L.; Sanguanmith, S.; Meesungnoen, J.; Causey, P.; Stuart, C. R.; Jay-Gerin, J.-P. *RSC Adv.* **2013**, *3*, 19282.

(77) Elliot, A. J.; Bartels, D. M. *The reaction set, rate constants and g-values for the simulation of the radiolysis of light water over the range 20 to 350 °C based on information available in 2008*; AECL Report No. 153-127160-450-001; Atomic Energy of Canada Limited: Chalk River, ON, 2009.

(78) Kuppermann, A. In *Actions Chimiques et Biologiques des Radiations*; Haïssinsky, M.; Ed.; Masson: Paris, 1961; vol. 5, pp. 85–166.

(79) Hummel, A. *Radiation Chemistry: The Chemical Effects of Ionizing Radiation and their Applications*; Interfaculty Reactor Institute-Technische Universiteit Delft (IRI-DUT): Delft, The Netherlands, 1995.

(80) At 25 °C, D = 2.2 × 10^{-9} m^2 s^{-1} for •OH, 2.3 × 10^{-9} m^2 s^{-1} for H_2O_2, 4.9 × 10^{-9} m^2 s^{-1} for e^-_{aq}, and 7 × 10^{-9} m^2 s^{-1} for H• (see **ref. 59**).

Figure captions

Figure 1:

Graphical representation of a possible mechanism that could help explain the "oxygen depletion hypothesis" in FLASH. FLASH-RT (right) induces a rapid depletion of oxygen, which – before reoxygenation can occur – leads to transient protective hypoxia with reduced deleterious reactive oxygen species (ROS) levels and normal tissue toxicity compared with CONV-RT (left).

Figure 2:

Illustration of the irradiation model used in this work with a pulse of six 300-MeV per nucleon irradiating $^{12}C^{6+}$ ions (LET ~ 11.6 keV/μm), which (randomly and simultaneously) impact perpendicularly to the water surface (*XZ* plane) within a circle with radius R_o = 0.1 μm. The figure shows a three-dimensional representation of the carbon ion tracks traversing through the water calculated from our IONLYS Monte Carlo code. All ions travel along the *Y*-axis over the entire track length chosen for the calculations (~10 μm). Energetic secondary electrons (δ rays), which define the so-called "penumbra", can also be seen surrounding the central track "cores".

Figure 3:

Time evolution of the yield of oxygen consumption $G(-O_2)$ (in molecule per 100 eV), obtained from our Monte Carlo multi-track chemistry simulations of the radiolysis of aerated water by 300-MeV per nucleon irradiating carbon ions (LET ~ 11.6 keV/μm) at 25 °C, over the interval of ~1 ps to 10 μs. The *N* values chosen to illustrate the dose-rate effects vary from 1 to 75. The concentration of dissolved O_2 used in the calculations is 0.25 mM.

Figure 4:

Time dependence of the extents $\Delta G(-O_2)$ of the main reactions that contribute to the consumption and formation of oxygen on the time scale of ~1 ps–10 μs, calculated from our Monte Carlo multi-track chemistry simulations of the radiolysis of aerated water by 300-MeV per nucleon carbon ions for N = 10 (panel A) and 75 (panel B), at 25 °C. Note that in the absence of SOD, the disproportionation reactions of $O_2^{\bullet-}$ and $HO_2^{\bullet}$ that give H_2O_2 and O_2 are much slower than reactions (5) and (6) (**refs. 52 and 56**) and therefore do not appear in the figure for the time period under consideration. The concentration of dissolved O_2 used in the simulations is 0.25 mM.

Figure 5:

Variation of the concentration of the consumed oxygen $[-O_2]$ (in mM) as a function of time in the interval ~1 ps–10 μs, obtained from Eqs. (9) and (10) for various values of N between 1 and 75, using the $G(-O_2)$ values calculated from our Monte Carlo multi-track chemistry simulations of the radiolysis of aerated water by 300-MeV per nucleon irradiating carbon ions (LET ~ 11.6 keV/μm) at 25 °C (see Fig. 3). Data for N = 75 correspond to a dose rate of ~10^{10} Gy/s in our model system.

Figure 6:

Time evolution of the yield of hydrogen peroxide, $G(H_2O_2)$, as obtained from our Monte Carlo multi-track chemistry simulations of the radiolysis of aerated (black lines) and deaerated (blue lines) water with 300-MeV per nucleon (LET ~ 11.6 keV/μm) irradiating carbon ions at 25 °C, in the interval ~1 ps–10 μs. The different values of N, namely, 1 (solid line), 5 (dashed line), 10 (dotted line), and 50 (dash-dotted line) illustrate the dose-rate effect. The concentration of dissolved O_2 used in the simulations is 0.25 mM.

Figure 7:

Time dependence of the concentration of hydrogen peroxide, [H_2O_2] (in mM), for some selected values of *N*, the "number of incident carbon ions per pulse", obtained from Eqs. (9) and (10) using the $G(H_2O_2)$ values calculated from our Monte Carlo multi-track chemistry simulations of the radiolysis of aerated water by 300-MeV per nucleon (LET ~ 11.6 keV/μm) irradiating carbon ions at 25 °C, in the interval ~1 ps–10 μs (see Fig. 6). Data for *N* = 75 correspond to a dose rate of ~10^{10} Gy/s in our model system.

FIGURE 1

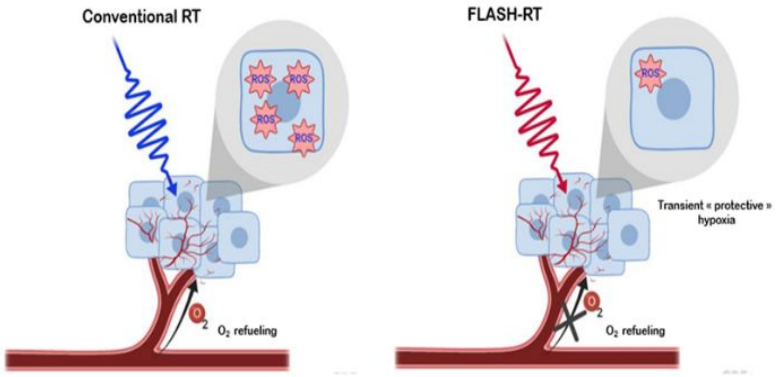

FIGURE 2

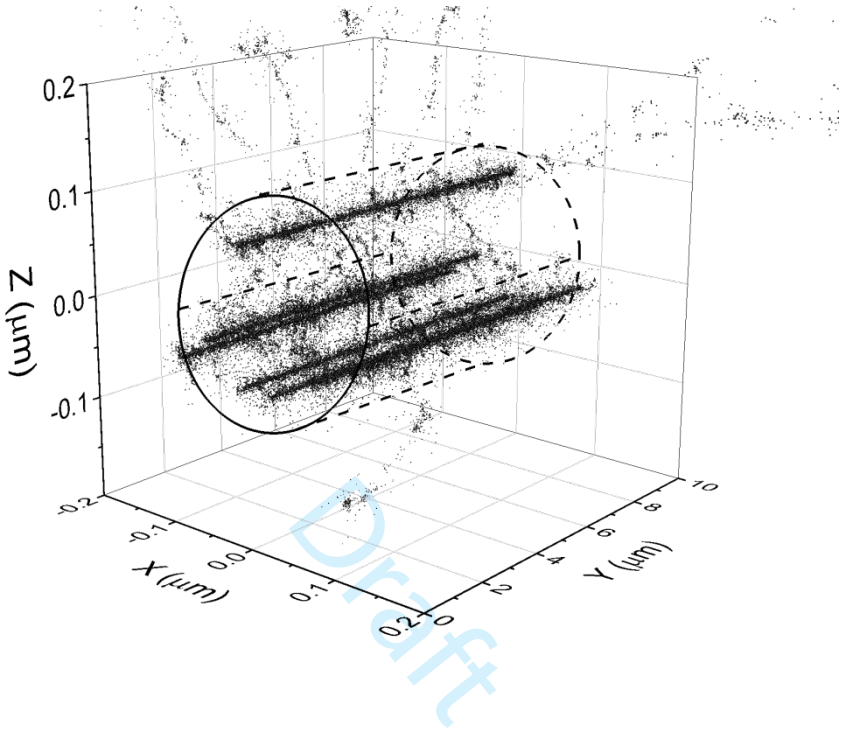

FIGURE 3

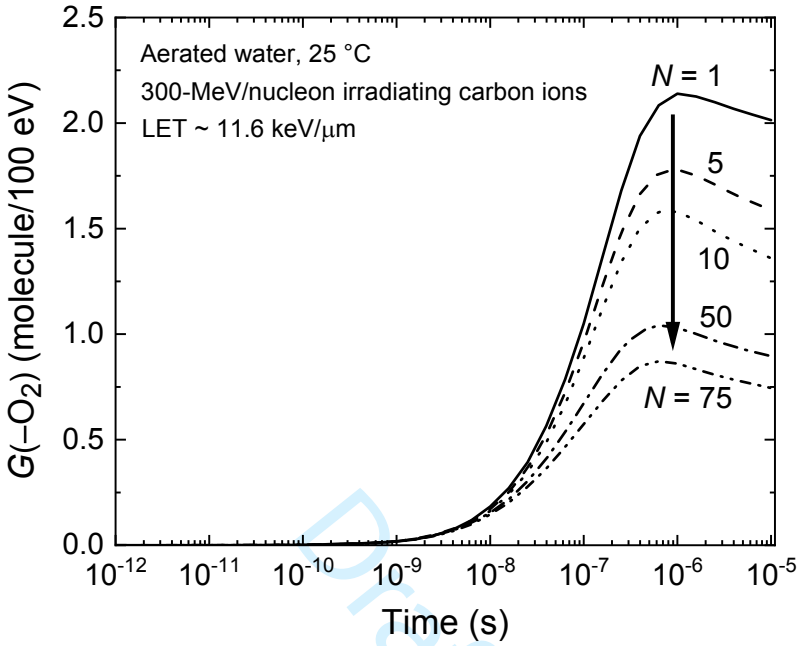

FIGURE 4

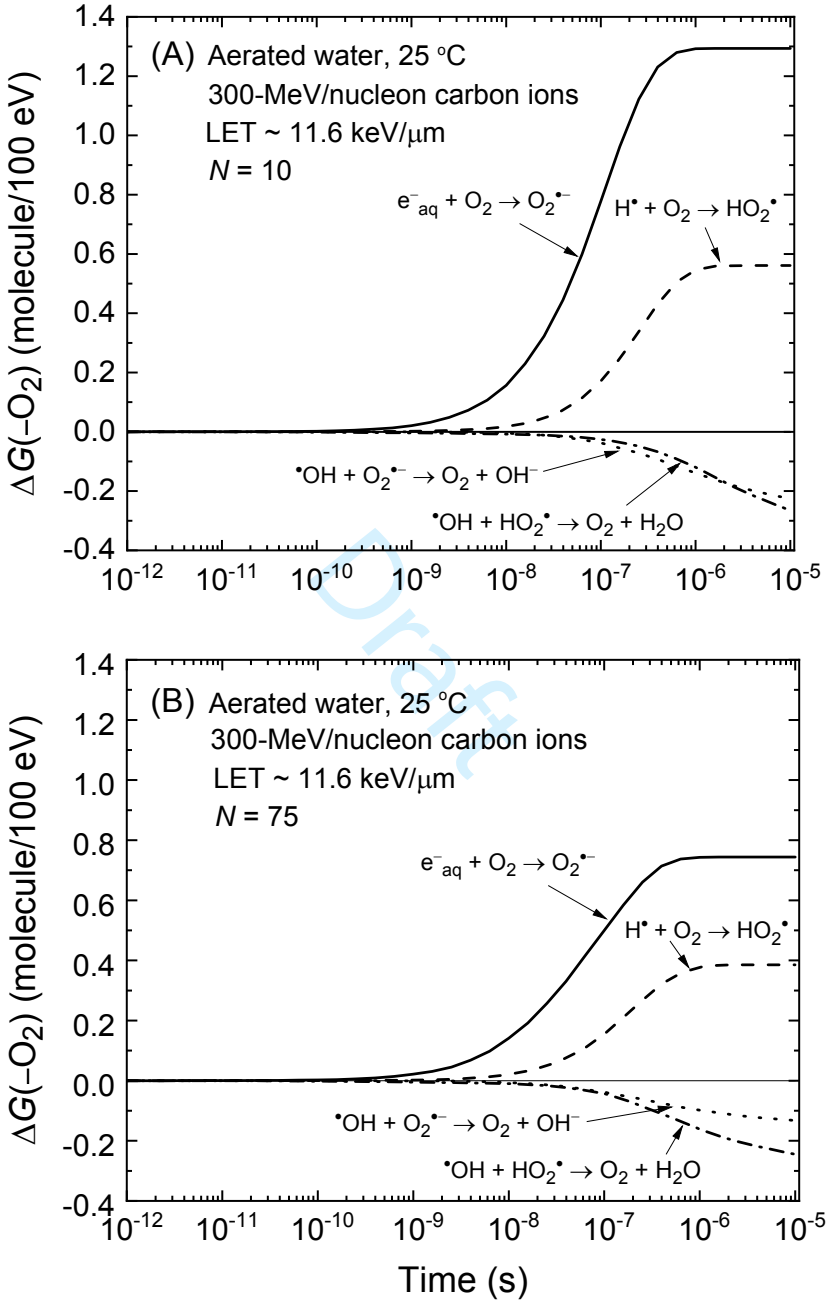

FIGURE 5

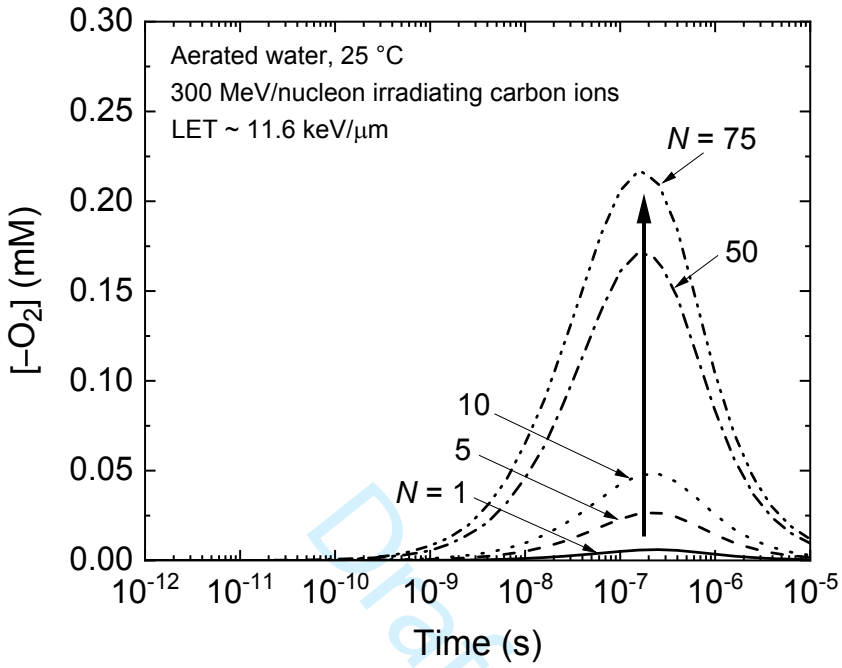

FIGURE 6

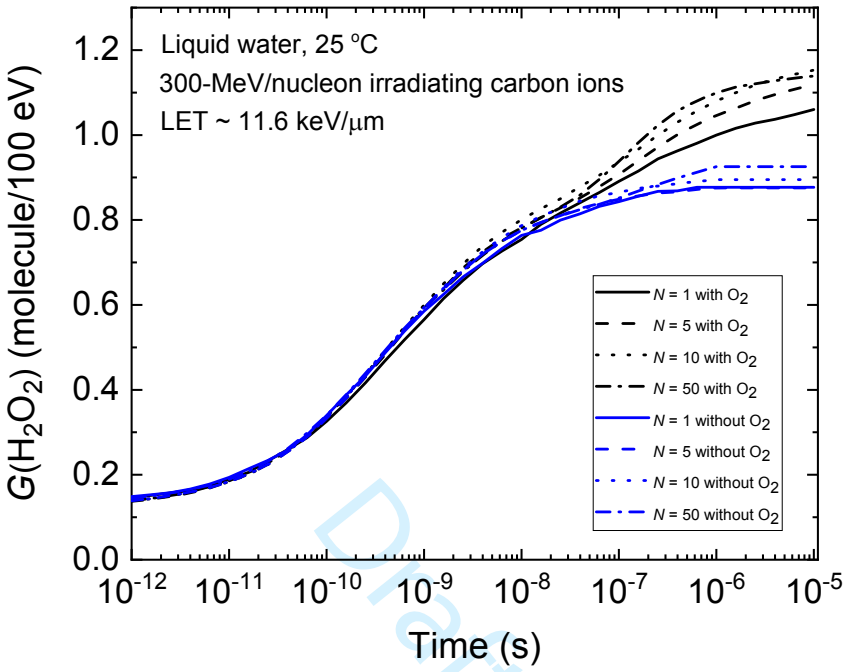

FIGURE 7